

The role of the gradient film properties in silica moisture barriers synthesized in a roll-to-roll Atmospheric Pressure Plasma Enhanced CVD reactor

Anna S. Meshkova,* Yaoge Liu, Fiona M. Elam, Sergey A. Starostin, Mauritius C. M. van de Sanden, Hindrik W. de Vries.

A. S. Meshkova, Y. Liu, F. M. Elam, Prof. M. C. M. van de Sanden, Dr. H. W. de Vries
DIFFER – Dutch Institute For Fundamental Energy Research
P.O. Box 6336, 5600 HH Eindhoven
The Netherlands
Email: a.meshkova@differ.nl

A. S. Meshkova, Y. Liu, F. M. Elam, Prof. M. C. M. van de Sanden
Plasma and Materials Processing Group
Department of Applied Physics
Eindhoven University of Technology
P.O. Box 513, 5600 MB Eindhoven
The Netherlands

F. M. Elam, Dr. S. A. Starostin
FUJIFILM Manufacturing Europe B.V.
P.O. Box 90156, 5000 LJ Tilburg
The Netherlands

Abstract

Silica-like films for moisture barriers were deposited on a polymeric substrate in an Atmospheric Pressure PECVD reactor using a $N_2/O_2/TEOS$ gas mixture. Statically deposited silica films were characterized by spatially resolved ATR FTIR and revealed a clear gradient in the silanol concentration. Silanol is an impurity in the silica network, resulting in pore formation, thus a higher silanol content leads to a decrease in the film density. Hence the spatial non-uniformity in the static profile results in a density gradient in the thickness of web-rolled films. The gradual transition from a lower to a higher density film appeared to be an essential requirement for maintaining the film integrity on the polymer. Hence, the porous layer acts as an adhesion promotion layer for the dense top layer. These optimal layer properties are achieved in a continuous single processing step.

Introduction

Over the past decades numerous applications of thin films have emerged in everyday life. The reason for the advancement in thin film technology is the broad range of useful film properties that can be accessed by understanding the thin film growth process. An example of such a functional film is an oxygen and water permeation barrier deposited on a polymer substrate. These functional films can be used in practical applications for the protection of flexible electronic components against exposure to moisture, like solar cells and quantum dots, but also for keeping food and medical packaging under controlled gaseous environments. [1]-[4]

Atmospheric Pressure Plasma Enhanced Chemical Vapor Deposition (AP-PECVD) has recently gained a lot of interest as a roll-to-roll compatible process to produce functional films. The small footprint and the absence of a complex and expensive vacuum system make the technology attractive from a technological and economic perspective. Thin silica films with excellent properties can be deposited by AP-PECVD using roll-to-roll processing. For example silica films with a Water Vapor Transmission Rate (WVTR) $< 6 \cdot 10^{-4} \text{ g m}^{-2} \text{ day}^{-1}$ (at 40 °C, 90% relative humidity) have recently been reported. [5]

Further improvement of the film quality as well as the throughput of the AP-PECVD process is an important industrial target. This target requires a detailed understanding of the plasma chemistry and the thin film growth mechanisms in the AP-PECVD reactor. In the “side fed” reactor, under investigation, the gas mixture is injected parallel to the electrodes (here from the left side of the electrodes), see **Figure 1**. The parallel gas injection between the cylindrical electrodes results in a reactive convective flow with a spatial deposition profile in the direction of the gas flow. [6] Several studies were carried out to characterize the local film properties in this reactor geometry by growing thin films without displacement of the substrate. [6]-[9]

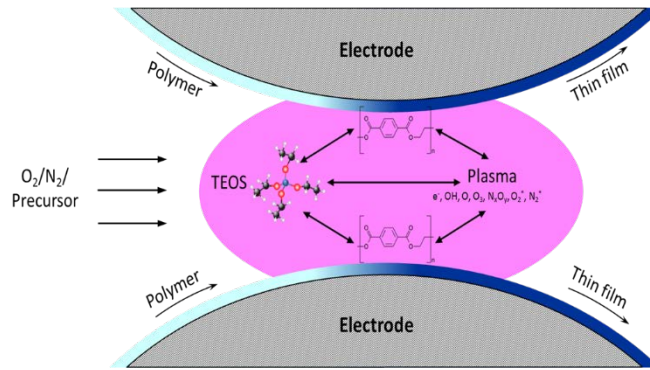


Figure 1 A schematic depiction of the electrode geometry (not to scale) from the side view of the roll-to-roll AP-PECVD reactor. In static mode the foil is not transported whereas in dynamic mode the foil is transported in the same direction as the gas flow.

Kakiuchi et al. ^[6] deposited thin films in an helium based atmospheric pressure plasma reactor using a VHF (150 MHz) source generating a power density of $20 \text{ W}\cdot\text{cm}^{-2}$. The film properties and thickness of silicon and silica films, under static deposition conditions, were studied as a function of the position in the reactor. The silicon layers were grown from silane (SiH_4). Due to the gradient properties of the silicon microstructure, the films were unsuitable for electronic devices demanding uniform electrical properties. The silica layers were deposited from the organosilicon precursor hexamethyldisiloxane (HMDSO). Spatially resolved FTIR indicated a variation in the carbon composition featuring a decrease in the carbon content for positions further away from the gas inlet position.

The growth mechanisms of silica thin films was also studied by Massines et al. ^[7] using a parallel plate Atmospheric Pressure Townsend Discharge (APTD). The properties of the films synthesized with $\text{N}_2\text{O}/\text{HMDSO}$ and $\text{N}_2\text{O}/\text{SiH}_4$ were compared. In the case of the SiH_4 precursor the density of the layer was influenced by particle formation in the plasma due to the high reactivity of SiH_4 . In both cases the chemical composition was comparable and silanol (Si-OH) bonds were present in the films regardless of the position in the reactor. Enache et al. ^[10] studied the growth rate profile experimentally in a gas mixture of $\text{N}_2\text{O}/\text{HMDSO}$, and compared the results to a fluid dynamics model.

Earlier research by Premkumar et al. ^[8] was carried out using a parallel plate AP-PECVD reactor in an Ar/N₂/O₂/HMDSO gas mixture using low duty cycle deposition conditions (0.25~4 W·cm⁻²). It was shown that the thickness profiles (precursor depletion rates) were influenced by the average discharge power. The silica films directly deposited on the bare polymer substrate were smooth and transparent at the gas inlet, followed by a region of powdery deposits. However, this powdery region was not observed when the polymer was protected by a thin silica (buffer) layer. Based on this study it was concluded that a powder-like coating was formed due to polymer etching of non-depositing active plasma species. A spatially resolved XPS study showed a constant over-stoichiometry of O/Si>2. This was attributed to the presence of silanol groups together with some carbon in the discharge effluent zone.

These earlier studies point to the formation of non-uniform film properties with respect to chemical composition and density. Hence a critical parameter in the film deposition process is the local deposition rate, which controls the flux of precursor fragments to the substrate, and their sticking probability. The precursor depletion along the gas flow via dissociation in the plasma as well as the drift-diffusion transport of the fragments results in a non-uniform deposition rate profile. The shape and properties of this deposition profile depend a.o. on the specific reactor geometry, type of precursor, gas flow rates and dissipated power in the plasma. The aim of this study is to understand how the film morphology and structure are influenced by the local deposition rate due to the non-uniform precursor depletion rate under moisture barrier deposition conditions using an industrially relevant cylindrical electrode geometry as reported by Starostin et al.^[1] Moreover, a better understanding of the non-uniform growth rate is obtained which is essential for the design of the reactor geometry, processing conditions and functional film properties in terms of adhesion and barrier performance.

Experimental Section

The films were deposited using a roll-to-roll AP-PECVD reactor. An elaborate description with a schematic representation of the AP-PECVD reactor used in this study was shown in a recent publication by Starostin et al.^[1] In short, the system consisted of a parallel bi-axial cylindrical electrode geometry, a gas injector and a foil transport system. Both electrodes were covered with polymeric foil which had two functions: as a dielectric barrier for the DBD system and as a substrate for deposition. Polyethylene-2,6-naphthalate (PEN) foil was used for the bottom electrode and a sacrificial foil (ASTERATM Functional Foils, AGFA PET) for the top electrode, which was transported at a constant line speed of $50 \text{ mm}\cdot\text{min}^{-1}$. Nitrogen gas was used as a carrier gas with a flow rate of 18 slm. Oxygen was used as the oxidizer of the tetraethylorthosilicate (TEOS) precursor for the silica layers. TEOS was diluted with 1 slm argon, and the reactant gas flows were kept constant at $1.8 \cdot 10^{-3}$ slm TEOS and 0.5 slm oxygen. A high voltage of approximately 2-3 kV was applied in a pulsed mode with 90 % Duty Cycle (DC) and the frequency ranged from 180-200 kHz. The dissipated power in the discharge was 575 W, corresponding to an approximate power density of $19.2 \text{ W}\cdot\text{cm}^{-2}$ (taking a characteristic discharge expansion length of 20 mm for the described experimental conditions). The radii of the drum electrodes were 120 mm. The discharge width was 15 cm and the smallest gaseous gap was 0.5 mm. Two types of deposition modes were adopted in this study. The ‘static mode’ when there was no foil displacement and deposition took place just within the discharge region, and the ‘dynamic mode’ when the foil was transported in the same direction as the gas flow and a uniform film thickness was deposited. In this study experimental conditions were selected based on previous work of dynamically deposited 100 nm thick films that resulted in a WVTR equal to $2 \cdot 10^{-3} \text{ g}\cdot\text{m}^{-2}\cdot\text{day}^{-1}$ and deposited in the full precursor depletion mode.^[1] It is known from previous work,^[1] that for the present experimental arrangement approximately 70% of the supplied gas flow was contributing to the deposition process. The gas loss can be attributed

to intentional “leaks” to secure the narrow gap ($\approx 100 \mu\text{m}$) between the gas injector and the polymer on the cylindrical electrodes. This paper concentrates on the study of static deposition profiles with the bottom electrode fixed. The statically deposited films were grown during 60 s of plasma exposure on a PEN substrate protected by a silica layer (to prevent interaction with the organic substrate) ^[8] and directly on the bare PEN substrate. The protective silica (buffer) layer was deposited at a precursor flow of $8.2 \cdot 10^{-3}$ slm and a web speed of $1 \text{ m} \cdot \text{min}^{-1}$, which resulted in a thin layer of 20 nm.

Film characterization

The variation of deposition rate along the gas flow direction was assessed by measuring the film thickness profile using a focused beam Spectroscopic Ellipsometry (SE). The spot size of the beam was $120 \mu\text{m}$ and the wavelength range was 245–1000 nm (M-2000D, J.A. Woollam Inc.). The SE was equipped with a translation table which allowed spatially resolved measurements of the static samples in the range of -20 mm to 20 mm over 641 points with a step of 0.1 mm. To describe the PEN substrate and the silica-like film, a Cauchy dispersion function was applied for both materials. The substrate anisotropy was not implemented into the model, ^[11] however the sample orientation was kept the same for each measurement. The ellipsometric data was analyzed using the J.A. Woollam Co. WVASE 32 software. The Mean Square Error (MSE) between the experimental data and the optical model was monitored.

Spatially resolved Attenuated Total Reflectance (ATR)-FTIR was performed on statically deposited silica-like films to clarify the role of local deposition rate on the film morphology.

This set-up utilized a Ge crystal with a 45° face angle and one internal reflection. The IR absorption spectra were acquired over 8 scans from 650 to 4000 cm^{-1} using the Perkin Elmer Frontier (Frontier FT-IR/FIR Spectrometer, PerkinElmer; Frontier UATR Ge/Ge, PerkinElmer). The spatial resolution of the crystal is 1 mm. Each absorption spectrum was determined by subtracting the bare substrate together with buffer layer spectrum and

background from the sample spectrum to remove interfering bands in the substrate and background. The penetration depth L of the evanescent wave can be determined with **Equation 1** below,^[12] where θ is the angle of incidence of the infrared light, λ is the wavelength in the crystal, n_1 is the refractive index of the crystal and n_2 the refractive index of the sample.

$$L = \frac{\lambda}{2\pi(n_1^2 \sin^2 \theta - n_2^2)^{1/2}} \quad (1)$$

The Ge crystal used in this research has a refractive index of 4.0. Silica film has a refractive index of approximately 1.5 and the angle of incidence was 45°. The calculated penetration depth according to **Equation 1** for the wavenumber region of 4000 – 3000 cm⁻¹ is 221 nm and 830 nm in the region of 1300 – 800 cm⁻¹. Deconvolution of all spectral peaks in the region of 4000 – 3000 cm⁻¹ was carried out by Peak Analyzer – Fit Peaks (Pro), OriginPro 9.1 in order to determine the absorbance intensity of each individual contribution of SiO-H and HO-H spectral peaks.

The surface morphology of the silica-like films was measured using Atomic Force Microscopy (AFM) (Park Systems NX10) in non-contact mode, using a tip with a radius of approximately 8 nm. In order to investigate the film morphology evolution, AFM images of 512x512 pixels were obtained with scanning areas of 2x2 μm². AFM images were analyzed by using GWYDDION software.^[13]

Interferometric Microscopy (IM) (Wyko NT9100 Optical Profiling System, Veeco Instruments Inc.) was carried out on the films to obtain larger field of view on the surface morphology, analyzing an area of 47×63 μm².

X-ray photoelectron spectroscopy (XPS) measurements were carried out using a Mg K_αX-ray source with a photon energy of 1253.6 eV (PHI 5500). The C1s, Si2p and O1s peaks were measured after a short sputter cleaning of the sample surfaces with an Ar ion beam.

A cross-cut tape adhesion test was performed on the silica samples in order to analyze the adhesive properties of the barrier layers in accordance with ISO 2409:2003. This test involved cutting a 5 by 5 grid over an area of 1 cm² through the silica layer using a special grid cutter and applying tape to the cut area. Glass fibre TQC High Performance Filament tape with a tensile strength of 7.6 N·cm⁻² (TQC, 2000) was used for the test. The tape was removed in one motion under an angle of approximately 60°. The crosscut samples were then examined under a microscope and the area of the remaining film is estimated for each of the squares. The method described may only be used as a pass/fail test and cannot be regarded as a quantitative measure of adhesion.

Results and Discussion

In the static deposition mode, the film thickness profiles and the local film morphology can provide valuable information about the precursor consumption as well as the main growth processes involved in AP-PECVD. The typical thickness profile of a film deposited in the static mode can be accurately resolved using the focused beam SE and is presented in **Figure 2**. The zero position on the x axis of the thickness profile corresponds to the smallest gap distance between the cylindrical electrodes. The thickness profile displays a very steep front growth starting at the position of -7 mm growing to almost 400 nm within a 1 mm distance.

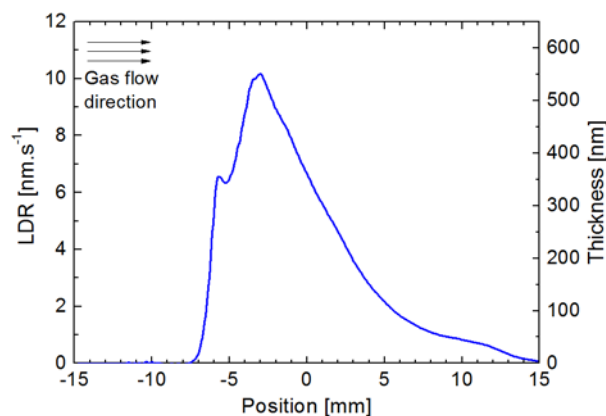


Figure 2 Local deposition rate (LDR) profile with respect to the position in the reactor at 90% DC.

As a result the thickness profile displays a high deposition rate before the zero position, followed by a decrease in the deposition rate caused by the precursor depletion. In addition, two distinct maxima can be observed in the deposition profile at 90% DC. The presence of two maxima suggests a difference in the transport kinetics of the precursor fragments arriving to the surface. This indicates that the fragmentation degree and density of the precursor molecules change in a very short time scale, causing non-uniformity in thickness and possibly also in the microstructure in the gas flow direction. Under these process conditions the deposition width is 22 mm, which also has consequences for the local gap distance. In the present experimental arrangement the minimum gaseous gap between the cylindrical electrodes is 0.5 mm but at the border of the discharge the gap distance is more than 1 mm. Therefore both electric field and local power density are non-uniform, while larger inter-electrode distance at the discharge peripheries may increase the probability of filament formation.

The earlier study in a parallel plate electrode geometry and lower power densities (up to $4 \text{ W}\cdot\text{cm}^{-2}$), ^[8] the film growth was less steep and the formation of the first maximum was assumed to originate from local electric field enhancement due to the relatively sharp electrode edge. Such a field enhancement is less likely in the case of the cylindrical electrodes. Despite the differences in electrode geometry, the power density and chemistry, and the general shape of the static deposition profile is similar to. ^[8]

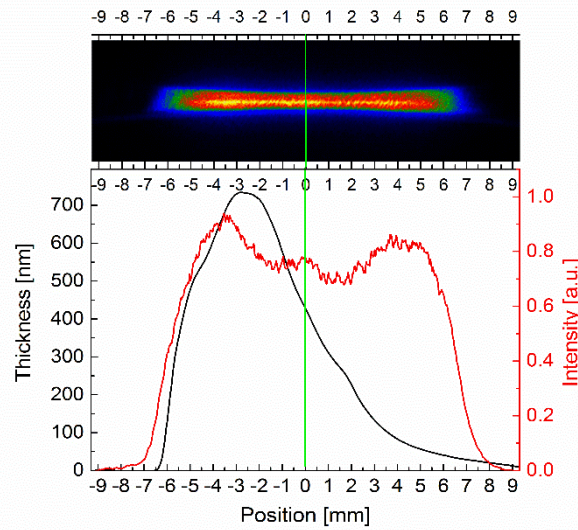


Figure 3 ICCD image of the discharge expansion at 50% DC and associated thickness profile measured with SE. The green line indicates the geometrical center of the electrodes. The colors in the integrated ICCD image reflect the spatial intensity of the discharge.

To correlate the dimension of the measured thickness profiles with the discharge expansion, an ICCD image in side view is obtained, ^[14] see **Figure 3**. The ICCD image of the discharge is integrated over multiple discharge events using an exposure time of 10 ms. To obtain a direct view on the discharge, the duty cycle is reduced to 50 % which is required to prevent edge instabilities normally counteracted at 90 % DC by a spacer. ^[14] The integrated intensity profile of the discharge is quite symmetric, and the gas flow with the depleting TEOS precursor only shows a small disturbance. The width of the discharge region is approximately 15 mm having a clear correlation with the associated thickness profile. The slight deviation in the onset of the thickness profile and the discharge intensity can be caused by an alignment error of the sample during the thickness measurement. For both a 50% and 90% DC, the static profiles are asymmetric with the deposition starting at the position of -7 mm, reaching a maximum thickness at around -3 mm. The tail end of the profile expands much further in the case of 90% DC (~15 mm) than in the case of 50% DC (~9 mm). This suggests that also the discharge expands further to around 15 mm in the case of 90% DC.

Film morphology

Previously it was shown that the porosity in the silica films is introduced by the presence of hydroxyl groups. [15]–[19] To investigate the influence of the local deposition rate on the film microstructure, spatially resolved ATR-FTIR was performed. [5] In **Figure 4** the ATR-FTIR spectra of the static profiles are shown at different positions along the gas flow direction in the regions of interest between 3000–4000 cm^{-1} and 1000–850 cm^{-1} .

The hydroxyl stretch region shows a change in the spectral feature at 2800–3700 cm^{-1} which is associated with the O–H vibration. This broad peak can be considered a superposition of three peaks: 1) at 3350 cm^{-1} associated with –OH from absorbed water in the film 2) at 3515 cm^{-1} attributed to associated silanol (a-SiO–H) groups and 3) at 3640 cm^{-1} attributed to isolated silanol (i-SiO–H) groups. [20], [21]

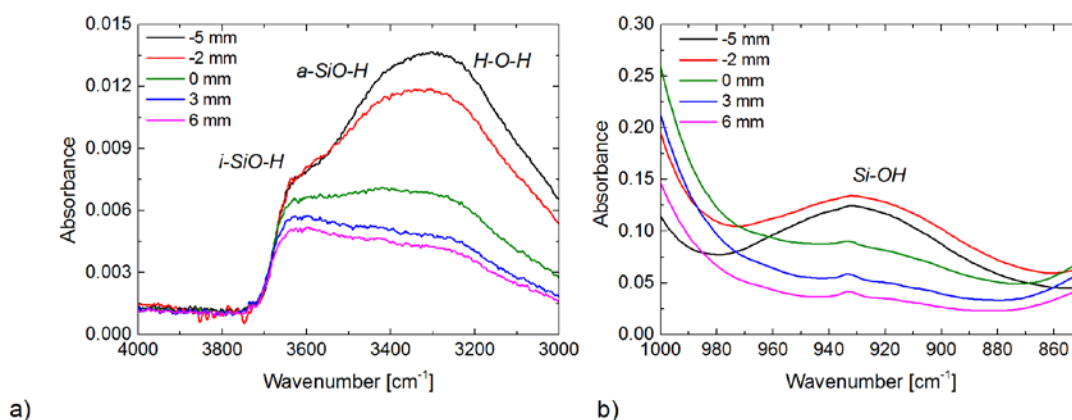


Figure 4 ATR-FTIR spectra of a silica-like film probed at different positions downstream in the gas flow direction in a) 3000–4000 cm^{-1} and b) 1000–850 cm^{-1} spectral regions. The positions of spectra represented in various colors refer to Figure 2.

The gradual decrease in the concentration of –OH groups is indicative of a decrease in the network porosity (increase in network density), which is particularly clear from the associated Si–OH groups. This prominent decrease in the silanol concentration in the static profile is not reported by other groups. [6], [7] The peak related to the silanol bond vibration at 930 cm^{-1} (Si–OH) displays the same gradual decrease in Si–OH density, see **Figure 4b**. The film

microstructure changes as a function of the position in the discharge. A shorter gas residence time results in higher network porosity, whereas a longer gas residence time results in denser films.

Deshmukh and Aydil reported in the case of low pressure PECVD, that a higher surface temperature and lower deposition rate is associated with a densification of the silica-like films via reduction of silanol groups in the layer.^[22] They concluded that water and SiOH species were formed as an intermediate surface reaction product, and subsequent reaction and elimination of the silanol species could become the surface limiting step when the deposition rate was too high. The surface limited growth is also observed by Starostin et al.^[1]

However, the role of homogeneous reactions cannot be excluded in the silanol formation, as shown in **Figure 4**. Taking two positions in the static profile at -5 mm and 0 mm, with the same local deposition rate of $6.5 \text{ nm}\cdot\text{s}^{-1}$, a clear drop in hydroxyl group concentration in the film is obtained. According to the study by Enache et al.^[10] the highest precursor concentration will not coincide with the maximum of the deposition rate profile because the precursor radicals created in the vicinity of the surface can directly stick to the surface, whereas the precursor radicals present in the bulk of the gas phase have to diffuse to the surface before sticking. This leads to a larger dissociation of the precursor and thus less silanol incorporation. This behavior is in good agreement with the variation in film microstructure observed in the downstream direction, assessed by spatially resolved ATR-FTIR analysis: higher network porosity for short gas residence time, and denser films deposited in longer residence time regions. **Figure 4** clearly illustrates that the absorbance of hydroxyl groups decreases in the downstream direction of the gas flow.

The XPS compositional analysis is listed in **Table 1**. All measured positions showed an O/Si ratio of approximately 2 with a barely detectable carbon level in the film. Hence, the films are inorganic and a variation in the stoichiometry with the position in the static profile that cannot

be resolved by XPS. However, ATR-FTIR measurement clearly indicates the subtle gradient changes in silanol concentration.

Table 1. Spatially resolved XPS compositional analysis of the static profile.

Position in the static profile, [mm]	Si [at. %]	O [at. %]	C [at. %]	O/Si
-5	32.90±0.99	67.01±2.01	0.00	2.04±0.04
0	33.19±0.99	66.51±1.99	0.03	2.0±0.04
4	33.68±1.01	65.95±1.98	0.01	1.96±0.04

The gradient properties in the film density of the static profile along the gas flow direction translate as a variation in the depth of the layer in the dynamically deposited film as shown in **Figure 5**. When the LDR profile is integrated over the deposition length along the electrode the actual growth front during dynamic deposition conditions can be deduced.

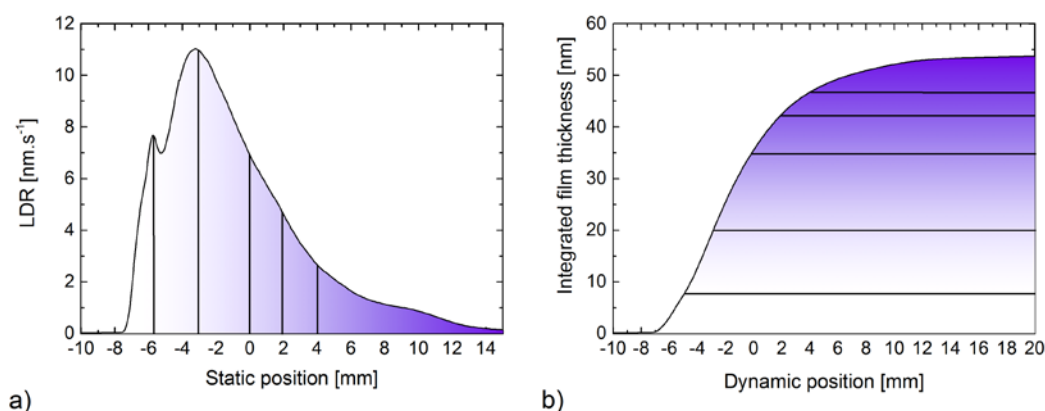


Figure 5 Integration of the local deposition rate profile translated into the film growth at the start of a dynamic profile: a) local deposition rate profile; b) growth profile of the film deposited in the dynamic mode assuming a line speed of 100 mm·min⁻¹ (integrated plot of the local deposition rate).

As mentioned, the O–H stretching region that occurs in the 4000 – 3000 cm⁻¹ range consists of three peaks; the isolated silanol peak at 3650 cm⁻¹, the neighboring silanol peak at 3450 cm⁻¹ and the H-OH stretch peak attributed to interaction with adsorbed water on the sample at 3250 cm⁻¹. [20], [21] Therefore deconvolution of these three components may provide a clearer

understanding of the individual contributions in the composite absorption peak observed between 4000 and 3000 cm^{-1} . The spectra depicted in **Figure 4** were deconvoluted and the absorbance of each individual hydroxyl stretch was portrayed as a function of the position in the static profile, see **Figure 6a** and as the relative thickness in the barrier layer film, see **Figure 6b**.

Figure 6b shows a reduction in the concentration of the network disrupting silanol groups as well as a reduction in the concentration of water trapped in the pores of the barrier layers deposited in the dynamic mode from the bottom (polymer interface) to the top (surface).

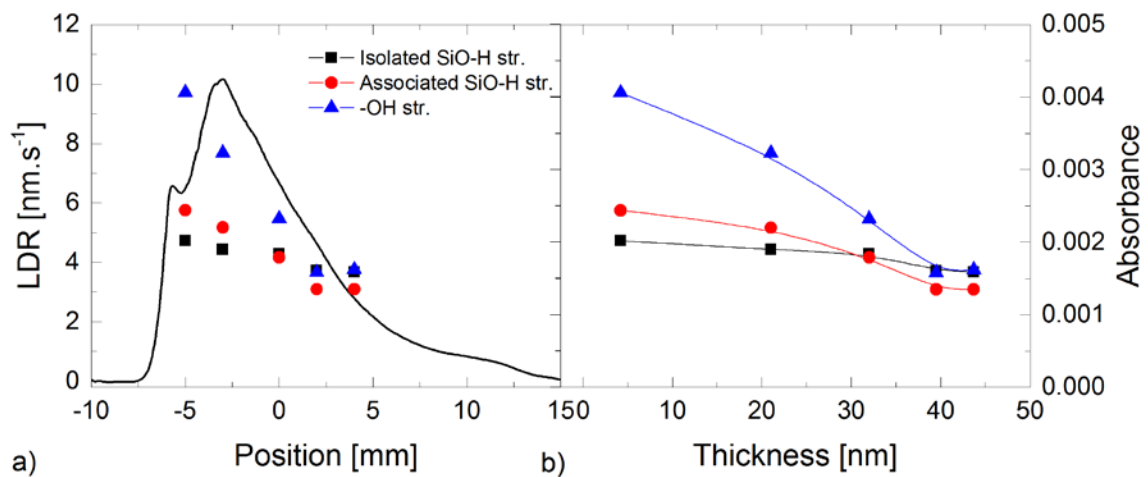


Figure 6 Deconvolution of the ATR-FTIR absorption spectra shown in Figure 4: a) Absorbance as a function of position in the reactor b) Absorbance as a function of the relative thickness of the samples if projected as a deposition in the dynamic mode with a line speed of 100 $\text{mm}\cdot\text{min}^{-1}$.

Moreover, the depth gradient properties of the silanol concentration with respect to the local film thickness of the silica layer can be derived. It should be noted that characterization of the film morphology of dynamically deposited films by ATR-FTIR will always probe an average value of the silanol concentration for the whole film thickness. ^[5]

By looking into trends from each individual hydroxyl stretch, the isolated SiO-H is almost constant throughout the film thickness. However, there is a clear decrease in the concentration

of associated silanol and the O-H stretch from the bottom to the top region of the film. The fact that the associated silanol shows the same trend as the O-H stretch indicates that the presence of these peaks are indicative for permeating channels. This also means that the probability of interconnected nanoporous permeation channels from the bottom to the top of the film decreases due to the presence of a thin and dense top-layer. From **Figure 6**, the thickness of the dense part of the silica layer is estimated to be approximately 10-15 nm assuming a line speed of $100 \text{ mm}\cdot\text{min}^{-1}$. The dense top-layer is deposited beyond the center position at relatively low LDR values of $1\text{-}3 \text{ nm}\cdot\text{s}^{-1}$. Interestingly this gradient transition from a porous layer facing the polymer to the gradually denser top-layer is always present and independent of the web speed.

Adhesion properties (polymer-film interface)

To understand the role of the intrinsically formed relatively porous layer, when the films are deposited in the dynamic mode, static profiles were deposited on a protective silica (buffer) layer and directly on the bare PEN substrate as shown in **Figure 7**. The thickness profile without the buffer layer is very similar to the profile of the film with the buffer layer up to 1 mm beyond the center of the electrodes. Further downstream the calculated layer thickness is very erratic with a large uncertainty, characterized by the Mean Square Error (MSE). Since the MSE represents the quality of the match between the ψ and Δ calculated from the model and the ψ and Δ from the experimental data, it can be concluded that the optical model in this region is not valid due to (local) variations in the film properties being the size of the wavelength of the light source.

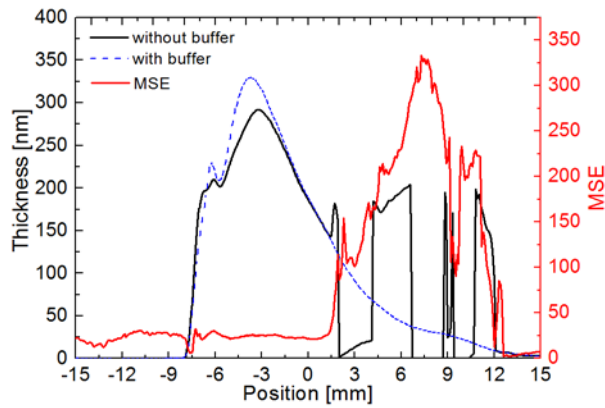


Figure 7 Thickness profile deposited in the static mode without a buffer layer in a solid black line, thickness profile deposited with a buffer layer depicted in dashed blue line. The red line is Mean Square Error (MSE).

The surface morphology of both static samples was studied by AFM. Different regions of the samples were compared as shown in **Figure 8**. First films deposited on bare PEN foil, and second films deposited on a pre-deposited protective buffer layer characterized by a high degree of porosity.

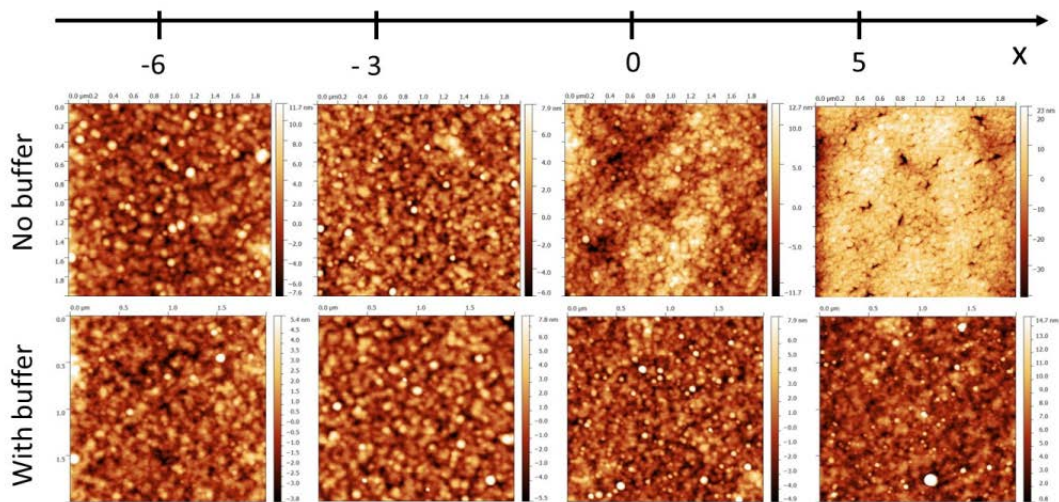


Figure 8 AFM micrographs of static samples deposited without a buffer layer (top images) and with a buffer layer (bottom). The indicated positions (x) refer to the static profile position shown in Figure 7.

The surface morphology of the film deposited on the protective layer is smooth and transparent without fissuring from the start to the end. However, the surface morphology of the films deposited on the bare polymer show many small fissures at the position of 2 mm and beyond. The discrepancy in the surface morphology with and without the protective layer clearly occurs after the center position and coincides with a strong increase in the MSE of the SE thickness calculation. Meanwhile the surface becomes cracked for the film deposited on the bare polymer. The visual appearance of the tail end region is hazy in comparison to the film deposited on the protective layer. However, from the AFM analysis no dust formation is observed on both thickness profiles. The change in the surface morphology suggests that the tail end part is delaminated from the polymer surface.

As earlier discussed, in the region of the tail end the silica layer has the highest degree of cross-linked Si-O-Si network, and thus it can be expected that this region of the film exhibits the highest level of brittleness and stress. In **Figure 9** a more detailed AFM analysis of the surface morphology of the film directly deposited on the polymer in the region from 2 to 9 mm is shown. The surface morphology of this region reveals wavy structures with a height difference of about 80 nm and regions with fissures having a size in the range of 20-100 nm.

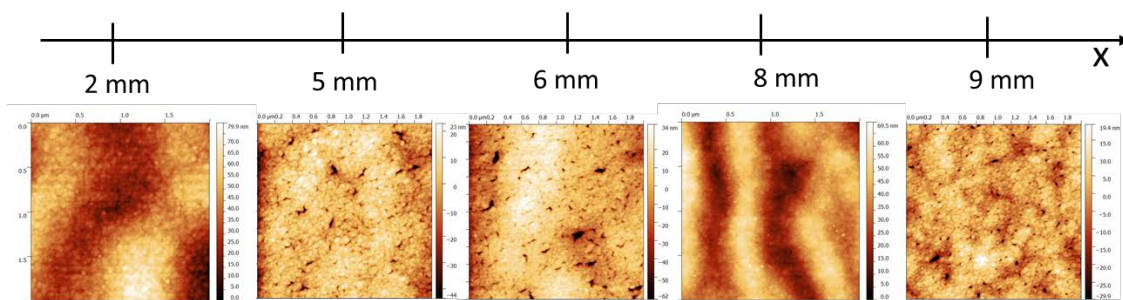


Figure 9 AFM micrographs of badly adhered region for the sample deposited without a buffer layer.

Additional surface analysis by Interferometric Microscopy confirms that the waviness of the silica layer determined by AFM extends over a large area, see **Figure 10**.

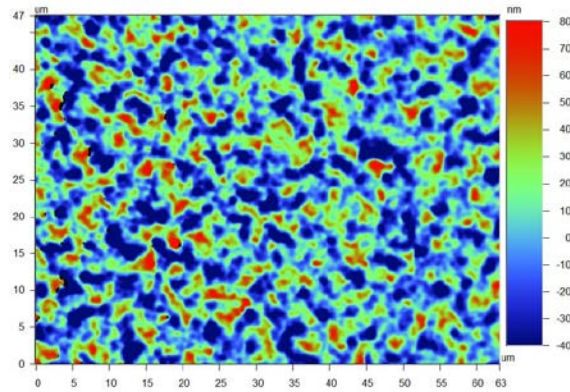


Figure 10 Surface morphology of a badly adhered region imaged by IM with a field of view of $47 \times 63 \mu\text{m}^2$.

Generally it is considered that compressive or tensile stresses in the films can cause fractures, delamination and buckling. Cui et al. [23] reported that parameters such as the deposition rate, exposure time in the plasma, the network structure of the layer and the density of the inorganic layer can significantly affect the adhesion of atmospheric plasma deposited films on polymeric substrates. They observed that the adhesion energy increased with decreasing film density, and they hypothesized an increased plasticity occurred due to molecular relaxation and rearrangement as well as increased flexibility of the Si-O-Si chains. [23]

From the spatially resolved ATR-FTIR it can be concluded that exactly in the region where the fissuring occurs, the film has the highest density and comprises the least flexible Si-O-Si chains. The stress relaxation may be induced by the fissuring of the layer as portrayed in the AFM micrographs of **Figure 9**. Similarly the wavy structure between positions 2-9 mm can be an indication of stress relaxation as the film is very loosely adhered to the polymeric substrate which can lead to the formation of a buckled structure. [24], [25]

To assess the adhesion properties a cross-cut tape adhesion test is performed on the statically deposited films both with and without a buffer layer.

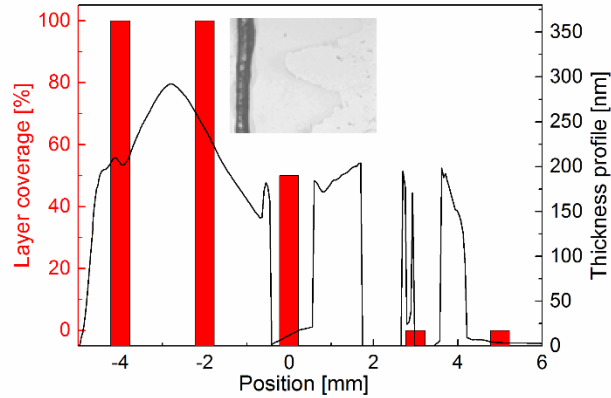


Figure 11 Qualitative indication of the layer coverage after a crosscut adhesion test on the static sample deposited without a buffer layer. The picture is made by optical microscopy of the border line between remaining layer and fully removed layer.

Optical microscopy reveals that the silica layer deposited without buffer layer is completely removed in the tail end region, and the silica layer is well adhered in the upstream region, see **Figure 11**. The edge of the silica film can also be seen in the inserted microscopic image. On the other hand, the static film profile deposited on the buffer layer exhibits excellent adhesion in any region of the profile. The adhesion improvement using an additional buffer layer was also observed for example by Cui et al. ^[26] Apart from the stress incorporated in the film due to the thermal expansion mismatch between the polymer and the dense silica layer, a competition between the interaction of oxygen radicals and the polymer (etching), and the flux of depositing species (deposition) cannot be excluded. ^[8] The plasma polymer interactions can induce a thin and weak boundary layer that can promote delamination of the silica layer. Hence, it can be concluded that complete mechanical destabilisation is observed in the precursor depleted region when a very dense silica film is deposited on a bare polymer substrate. An adhesion layer deposited at higher local deposition rate ($10 \text{ nm}\cdot\text{s}^{-1}$) is required to promote adhesion of the dense layer to the polymer. In fact, the adhesion layer, or buffer layer, can bridge the stress between the polymer and the dense silica layer. Moreover, the higher local deposition rate may prevent the formation of a weak boundary layer due to excessive plasma

polymer interactions. The deposition of a dynamically grown silica film will thus always lead to the formation of a porous well adherent layer between the polymer and the dense barrier top-layer.

Conclusion

The gradient film properties of static silica layers synthesized in an Atmospheric Pressure PECVD reactor were studied using spatially resolved ATR-FITR analysis. A variation in the film microstructure has been observed within the discharge region; with higher network porosity for a short gas residence time, while denser layers were deposited in the region with a longer gas residence time. This observation is particularly relevant for the architecture of the functional deposition, because within the discharge region these variable film properties translate into a gradient in the dynamically deposited films. This could provide the means to control the properties of the layers, such as the network porosity, which has a direct correlation with the barrier properties of the films. In a 50 nm thick silica layer only the top 10-15 nm most likely contributes to good moisture barrier properties.

Comprehensive AFM analysis of the static profiles and cross-cut adhesion testing revealed that a direct deposition on the polymer of a well crosslinked and dense SiO₂ film exhibited poor adhesion properties, probably due to stress build up and consequent delamination of the film. A good adhesion can be achieved by using a relatively porous layer as a compensation or buffer to provide an interface between the bare PEN and the dense silica film.

In our case, an adhesion promotion layer is automatically formed between the polymer and a dense top-layer. The gradient film properties, thus inherently grown in the AP-PECVD process, incorporate a film that enables good adhesion as well as good moisture and oxygen barrier properties. A single step deposition process can thus produce dual layer functionality.

In the dynamic deposition mode when uniform films are deposited, the gradient in the film properties are difficult to resolve. A comprehensive analysis of the static profiles by spatially

resolved ATR-FTIR provides a better understanding of the film morphology along the film depth. This approach is very suitable to investigate the role of specific precursors, gas flows and electrode geometry in optimizing the desired film properties.

Acknowledgements: The presented study was performed in the frame of the Industrial Partnership Programme i31 (APPPF) that is carried out under an agreement between FUJIFILM Manufacturing Europe B.V. and FOM, which is part of the Netherlands Organisation for Scientific Research (NWO), grant number FOM-13.0031/D. The authors would like to thank Bart van Loon for detailed film analysis by ATR-FTIR and focused beam SE. The authors are also grateful to dr. Jan Petersen (Fraunhofer IST) for XPS measurements and Rinie van Beijnen and Emile Gommers (FUJIFILM Manufacturing Europe B.V., Tilburg, The Netherlands) for their technical assistance.

Received: ((will be filled in by the editorial staff)); Revised: ((will be filled in by the editorial staff)); Published online: ((please add journal code and manuscript number, e.g., DOI: 10.1002/ppap.201100001))

Keywords: atmospheric pressure dielectric barrier discharges; non-uniform deposition rate, silica-like thin films; encapsulation films; roll-to-roll reactors

- [1] S. A. Starostin, M. Creatore, J. B. Bouwstra, M. C. M. van de Sanden, H. W. de Vries, *Plasma Process. Polym.* **2015**, *12*, 545.
- [2] L. Bárdos, H. Baránková, *Thin Solid Films* **2010**, *23*, 6705.
- [3] D. Pappas, *J. Vac. Sci. Technol. A* **2011**, *29* (2), 20801–1.
- [4] D. Merche, N. Vandencastele, F. Reniers, *Thin Solid Films* **2012**, *13*, 4219.

- [5] F. M. Elam, S. A. Starostin, A. S. Meshkova, B. C. A. M. van der Velden-Schuermans, J. B. Bouwstra, M. C. M. van de Sanden, H. W. de Vries, *Plasma Process. Polym.* **2017**, e1600143. DOI 10.1002/ppap.201600143.
- [6] H. Kakiuchi, H. Ohmi, T. Yamada, S. Tamaki, T. Sakaguchi, *Phys. Status Solidi* **2015**, 7, 1571.
- [7] F. Massines, N. Gherardi, A. Fornelli, S. Martin, *Surf. Coatings Technol.* **2005**, 200, 1855.
- [8] P. A. Premkumar, S. A. Starostin, H. W. de Vries, R. M. J. Paffen, M. Creatore, T. J. Eijkemans, P. M. Koenraad, M. C. M. van de Sanden, *Plasma Process. Polym.* **2009**, 6, 693.
- [9] S. A. Starostin, A. Meshkova, F. M. Elam, M. C. M. Van De Sanden, J. B. Bouwstra, H. W. De Vries, "Scaling of the atmospheric pressure DBD assisted deposition process for gas diffusion barrier film," presented in 22nd ISPC, July **2015**.
- [10] I. Enache, H. Caquineau, N. Gherardi, T. Paulmier, L. Maechler, F. Massines, *Plasma Process. Polym.* **2007**, 4, 806.
- [11] G. Aresta, P. A. Premkumar, S. A. Starostin, H. De Vries, M. C. M. Van De Sanden, M. Creatore, *Plasma Process. Polym.* **2010**, 7, 766.
- [12] N. J. Harrick, *J. Phys. Chem.* **1960**, 64, 1110.
- [13] D. Nečas, P. Klapetek, *Open Phys.* **2012**, 10, 181.
- [14] S. A. Starostin, S. Welzel, Y. Liu, B. van der Velden-Schuermans, J. B. Bouwstra, M. C. M. van de Sanden, H. W. de Vries, *Eur. Phys. J. Appl. Phys.* **2015**, 71, 20803.
- [15] W.A. Pliskin, *J. Vac. Sci. Technol.* **1977**, 14, 1064.
- [16] J. Schafer, R. Foest, A. Quade, A. Ohl, K. -D. Weltmann, *Plasma Process. Polym.*

- 2009**, 6, S519.
- [17] A. Brunet-Bruneau, J. Rivory, B. Rafin, J. Y. Robic, P. Chaton, *J. Appl. Phys.* **1997**, 82, 1330.
- [18] S. C. Deshmukh, E. S. Aydil, *Appl. Phys. Lett.* **1994**, 65, 3185.
- [19] P. Innocenzi, *J. Non-Crystallin. Solids.* **2003**, 316, 309.
- [20] J. Petersen, J. Bardon, A. Dinia, D. Ruch, N. Gherardi, *ACS Appl. Mater. Interfaces* **2012**, 4, 5872.
- [21] C. Vallee, A. Gouillet, A. Granier, A. van der Lee, J. Durand, C. Marliere, *J. Non-Cryst. Solids.* **2000**, 272, 163.
- [22] S. C. Deshmukh, E. S. Aydil, *J. Vac. Sci. Technol. A* **1995**, 13, 2355.
- [23] L. Cui, A. Ranade, M. A. Matos, L. S. Pingree, T. J. Frot, G. Dubois, and R. H. Dauskardt, *ACS Appl. Mater. Interfaces* **2012**, 4, 6587.
- [24] Y. Leterrier, *Prog. Mater. Sci.* **2003**, 48, 1.
- [25] Y. Leterrier, A. Mottet, N. Bouquet, D. Gillieron, P. Dumont, A. Pinyol, L. Lalande, J.H. Waller, J. -A. E Manson, *Thin Solid Films* **2010**, 519, 1729.
- [26] L. Cui, K. Lioni, A. Ranade, K. Larson-Smith, G. J. M. Dubois, and R. H. Dauskardt, *ACS Nano* **2014**, 8, 7186.

Graphical Abstract

Roll-to-roll synthesis of silica moisture barrier films with good adhesion properties to a polymer substrate can be obtained by forming a vertical gradient in the microstructure. It was found that a single atmospheric pressure plasma enhanced CVD processing step results in a dense top layer with good moisture barrier properties and a relatively porous bottom layer acting as an adhesion layer between the dense barrier layer and the polymer substrate.

Anna S. Meshkova,* Yaoge Liu, Fiona M. Elam, Sergey A. Starostin, Mauritius C. M. van de Sanden, Hindrik W. de Vries.

The role of the gradient film properties in silica moisture barriers synthesized in a roll-to-roll Atmospheric Pressure Plasma Enhanced CVD reactor

